

MATERIALS SCIENCE

Sustaining enhanced condensation on hierarchical mesh-covered surfaces

Rongfu Wen^{1,2}, Shanshan Xu², Dongliang Zhao², Lixin Yang³, Xuehu Ma⁴, Wei Liu^{1,*}, Yung-Cheng Lee² and Ronggui Yang^{2,*}

ABSTRACT

Controlling the solid–liquid–vapor tri-phase interface is of fundamental importance for a broad range of industrial applications including biomedical engineering, energy production and utilization, environmental control, water production, and thermal management. Although a lot of progress has been made over the past few decades on surface manipulation for promoting droplet removal, it is challenging to accelerate both droplet growth and surface refreshing for enhancing vapor-to-liquid condensation. Here we present a superhydrophobic hierarchical mesh-covered (hi-mesh) surface to enable continuous sucking flow of liquid condensate, which achieves fourfold-higher droplet growth and 36.8% faster surface refreshing compared to the state-of-the-art dropwise condensation. Unprecedented enhanced condensation heat transfer is observed to be sustained over a wide range of surface subcooling on the hi-mesh surfaces. This demonstration of sustained enhanced condensation enhancement is not only of fundamental scientific importance, but also provides a viable strategy for large-scale deployment of micro/nanostructured surfaces in a diverse range of technologies.

Keywords: condensation, hierarchical mesh, sucking flow, droplet dynamic, water-repellency, heat transfer enhancement

INTRODUCTION

The control of surface–liquid interactions is exploited in nature [1–4] and is playing an increasingly important role in various technologies, such as spraying, printing, biomedical engineering, water harvesting, thermal management, and energy production [5–9]. Liquid behaviors on a surface can range from complete spreading, e.g. tears of wine, to minimal wetting, e.g. the superhydrophobic lotus leaf. Inspiration from nature [10–13], such as lotus leaves, water striders, and butterfly wings, has led to the development of water-repellent surfaces that rely on the formation of a stable air–liquid interface between the liquid and solid surfaces [14–17]. Although a lot of progress has been made on micro/nanostructured surface design with spectacular water-repellency, droplets can nucleate and grow within the surface structures rather than at the top, with a size comparable to that of the surface features, when such a cold water-repellent surface is exposed to a humid environment [18–20]. The

nucleation-induced pinned droplets greatly inhibit surface refreshing and destroy the water-repellency of micro/nanostructured surfaces, which makes it challenging to apply them to many industrial applications including anti-fogging, anti-icing, water harvesting, and humidity control of the built environment [19,21].

For any of these, controlling vapor-to-liquid condensation is of fundamental interest. It also plays an essential role in the efficiency of various energy-intensive industrial technologies including power generation, energy utilization, water desalination, air-conditioning, and thermal management of electronics [22,23]. It is well known that dropwise condensation on hydrophobic surfaces (Fig. 1A), where the frequent roll-off of condensed droplets, e.g. on a vertical surface due to gravity, helps to refresh the surface that is exposed to the vapor, has an order of magnitude higher heat transfer efficiency than that of filmwise condensation on hydrophilic surfaces (Fig. 1B). Promoting dropwise condensation

¹School of Energy and Power Engineering, Huazhong University of Science and Technology, Wuhan 430074, China;

²Department of Mechanical Engineering, University of Colorado, Boulder, CO 80309, USA; ³School of Mechanical, Electronic and Control Engineering, Beijing Jiaotong University, Beijing 100044, China and ⁴State Key Laboratory of Fine Chemicals, Liaoning Key Laboratory of Clean Utilization of Chemical Resources, Institute of Chemical Engineering, Dalian University of Technology, Dalian 116024, China

*Corresponding authors: E-mails: w.liu@hust.edu.cn; ronggui.yang@colorado.edu

Received 21 July 2018; Revised 27 August 2018; Accepted 3 September 2018

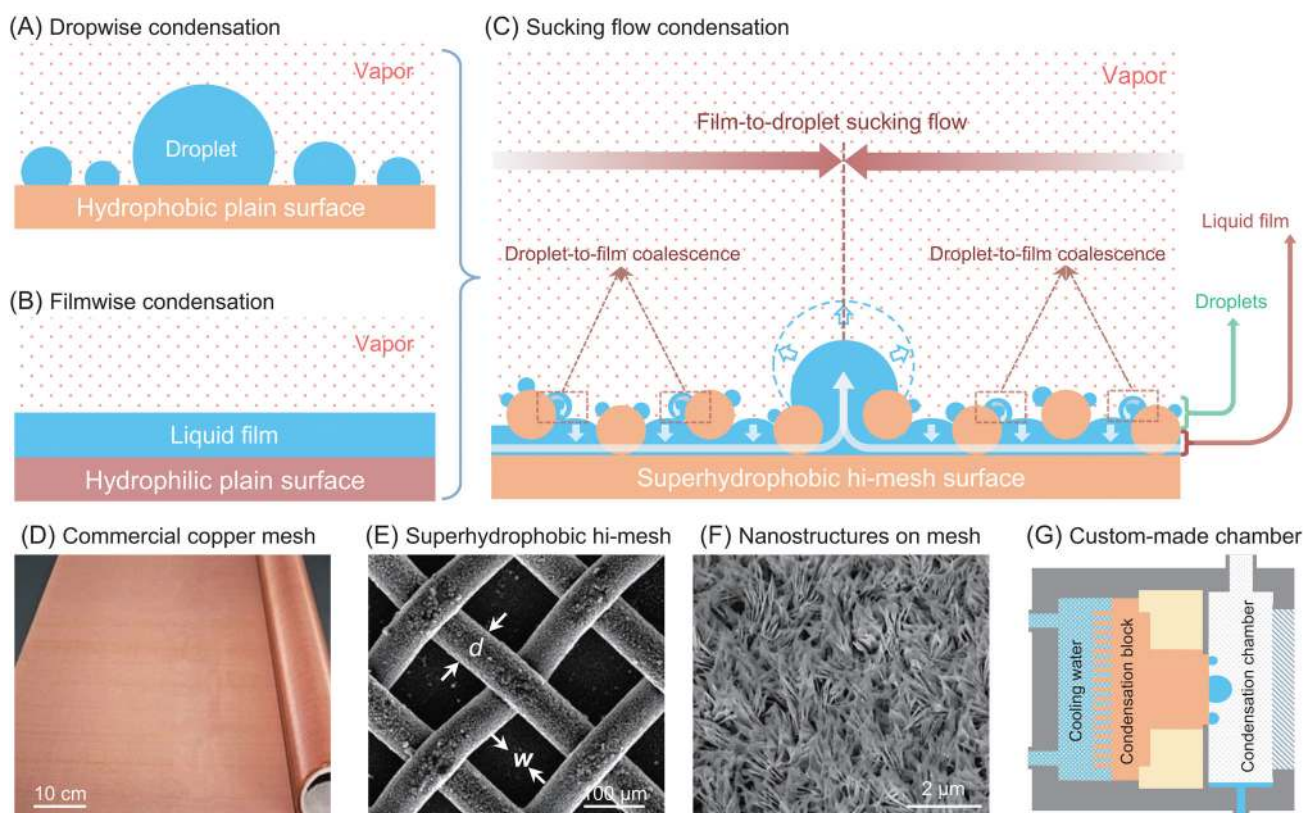


Figure 1. Hierarchical mesh-covered (hi-mesh) surfaces. (A) Dropwise condensation on a hydrophobic plain surface that is covered by discrete droplets. (B) Filmwise condensation on a hydrophilic plain surface that is covered by a continuous liquid film. (C) Sucking flow condensation on a hi-mesh surface consisting of droplet-to-film coalescence and film-to-droplet sucking flow for efficient surface refreshing and droplet growth. The thin liquid film between the substrate and woven mesh layer provides interconnected channels for sucking flow. (D) Commercial woven copper mesh used to develop hi-mesh surfaces. (E) Scanning electron microscopy (SEM) image showing the hi-mesh surface consisting of woven copper mesh wires bonded onto a copper substrate. (F) SEM image showing the high-density copper oxide nanostructures covering the mesh wires and substrate. (G) Schematic of the custom-made condensation chamber showing the vertically mounted test surfaces.

by surface modification has thus been of great interest since its discovery [24–31]. However, the long-standing challenge for better heat transfer performance is to improve both surface refreshing and droplet growth [23,28,29]. Compared to water-repellent nanostructured materials for self-cleaning and anti-fogging [21,32,33], it is extremely challenging to create large-area structured surfaces cost-effectively on metals with high thermal conductivity to fulfill both fluid mechanics and thermal requirements. Metallic micro-networks with interweaving liquid channels, such as copper micro-meshes and micro-foams, have been widely exploited in various industrial applications including oil–water separation and catalyst support medium [34,35] due to their low cost and good scalability. These copper meshes and foams have also been used to improve liquid wicking for high-heat-flux boiling and evaporation heat transfer [23,36]. Although we briefly reported an interesting condensation phenomenon on woven mesh in a recent study [37], a systematic study on the fundamental mechanism is still lacking.

Here, we present a superhydrophobic hierarchical mesh-covered (hi-mesh) surface that can be scalably manufactured using low-cost woven copper micro-meshes, to enable sucking flow condensation for expediting both droplet growth and surface refreshing, as shown in Fig. 1C. In this work, commercially available woven copper meshes (Fig. 1D) with a wire diameter d of 65 μm and spacing widths w of 65, 130, and 195 μm (corresponding to $w/d = 1, 2, \text{ and } 3$) are used as the starting materials. The typical structural features of the hi-mesh surfaces are formed by bonding a woven copper mesh onto the plain copper substrate using a thermal diffusion approach (Fig. 1E). The thickness of the bonded woven mesh layer is about 85–98 μm , measured by a micrometer. The bonding quality between the substrate and the mesh layer can affect the sucking flow condensation performance, due to the variations in the interface thermal resistance between the substrate and mesh layer, the flow resistance and the thermal resistance of the liquid film. High-density knife-like copper oxide nanostructures, ~ 10 nm in

tip, $\sim 1 \mu\text{m}$ in height, and 200–400 nm in pitch, are formed on all the exposed surfaces of the substrate and mesh wires (Fig. 1F) by the self-limiting chemical oxidization method (detailed surface fabrication and characterization are given in Supplementary Note S1, available at *NSR* online). These nanostructures serve as nucleation sites for droplet formation and growth. Between the substrate and the woven mesh layer, there are plenty of interconnected channels (microgaps) providing liquid condensate flow passages. Mesh wires form lots of micropores that are directly connected with the microgaps (interweaving channels), which can serve as outlets for draining the thin film liquid condensate in the microgaps. During vapor condensation, the nucleated droplets on the substrate rapidly grow and coalesce to form a thin liquid film in the interconnected channels between the substrate and woven mesh layer. When small droplets growing on the mesh wires merge with the thin liquid film, they can be efficiently removed by being pulled into the liquid film, accelerating surface refreshing for droplet re-nucleation and growth on the mesh wires. With continuous droplet-to-film coalescence, the interweaving channels can be filled with liquid condensate. Once the liquid film overcomes the Laplace pressure and grows out of the woven mesh layer, the surrounding liquid condensate that is accumulated in the interweaving channels can be continuously drawn out in the form of gravity-driven falling droplets due to the interconnected liquid film, resulting in rapid surface refreshing (a detailed analysis is given in Supplementary Note S2, available at *NSR* online). By coupling the high-performance dropwise condensation on mesh wires and thin liquid film condensation in the interweaving channels, the sucking flow condensation provides an effective approach to improve droplet growth and surface refreshing simultaneously, which could outperform both filmwise and dropwise condensation performance.

To demonstrate the sucking-flow-enhanced condensation, we measure the condensation characteristics on the superhydrophobic hi-mesh surfaces through optical visualization experiments using a custom-made condensation test chamber (Fig. 1G), where the test surfaces are vertically mounted (a detailed description of the experimental system is given in Supplementary Note S3, available at *NSR* online). Condensation heat transfer experiments on other superhydrophilic, hydrophilic, hydrophobic, and superhydrophobic surfaces are also conducted for comparison. All experiments are performed at the water vapor pressure of $60 \pm 0.5 \text{ kPa}$, which are the common vacuum conditions for thermal desalination, low-temperature heat pumps, heat pipes and high-efficiency industrial condensers

[23,38]. Throughout the condensation experiments, the chamber pressure and temperature are continuously monitored to ensure stable condensation conditions. The concentration of non-condensable gases in the condensation chamber is $\sim 2.5\%$. As the driving force for condensation, surface subcooling is defined as the temperature difference between the vapor temperature and surface temperature. The surface temperature is independently controlled via a water cooling loop where the inlet and outlet temperature of the cooling water is measured to determine the condensation heat flux and heat transfer coefficient. The uncertainties of the heat transfer data are calculated from the measurement uncertainties via the error propagation method (a detailed data reduction is given in Supplementary Note S4, available at *NSR* online). Dropwise condensation on the vertical surfaces occurs through repeated droplet cycles of nucleation, growth, coalescence, and departure. New droplets nucleate on a refreshed area after the coalescence and removal of old droplets. Due to the self-similarity of dropwise condensation [38], the steady-state condensation heat transfer performance can be evaluated through the statistical analysis of transient droplet behaviors. Here the droplet behaviors ($> 20 \mu\text{m}$) over a duration of 60 s in a field of view of $4 \text{ mm} \times 4 \text{ mm}$ on the test surfaces are recorded.

RESULTS AND DISCUSSION

Considering the dependence of droplet behaviors on surface subcooling, we first quantitatively characterized the droplet dynamics under small surface subcooling ($\Delta T < 4.5 \text{ K}$; details are given in Supplementary Note S5, available at *NSR* online). For ‘conventional’ dropwise condensation on a plain hydrophobic surface, the falling of the droplets off the vertical surface is driven by gravity (Fig. S5A, also Movie S1). However, the superhydrophobic nano surface is covered with high-density small condensed droplets where droplet jumping plays the most important role in droplet removal (Fig. S5B, also Movie S2). Compared to the hydrophobic plain and superhydrophobic nano surfaces, three kinds of droplet jumping modes are observed on the superhydrophobic hi-mesh surfaces (Fig. S5C, also Movie S3): coalescence-induced droplet jumping on mesh wires, self-jumping of a single droplet in micropores, and mixed jumping of droplets inside and outside of micropores (Fig. S5D–F). As a result, the departure radii of the droplets on the superhydrophobic nano and hi-mesh surfaces are greatly decreased, compared to those on the hydrophobic plain surface (Fig. S5G). A larger

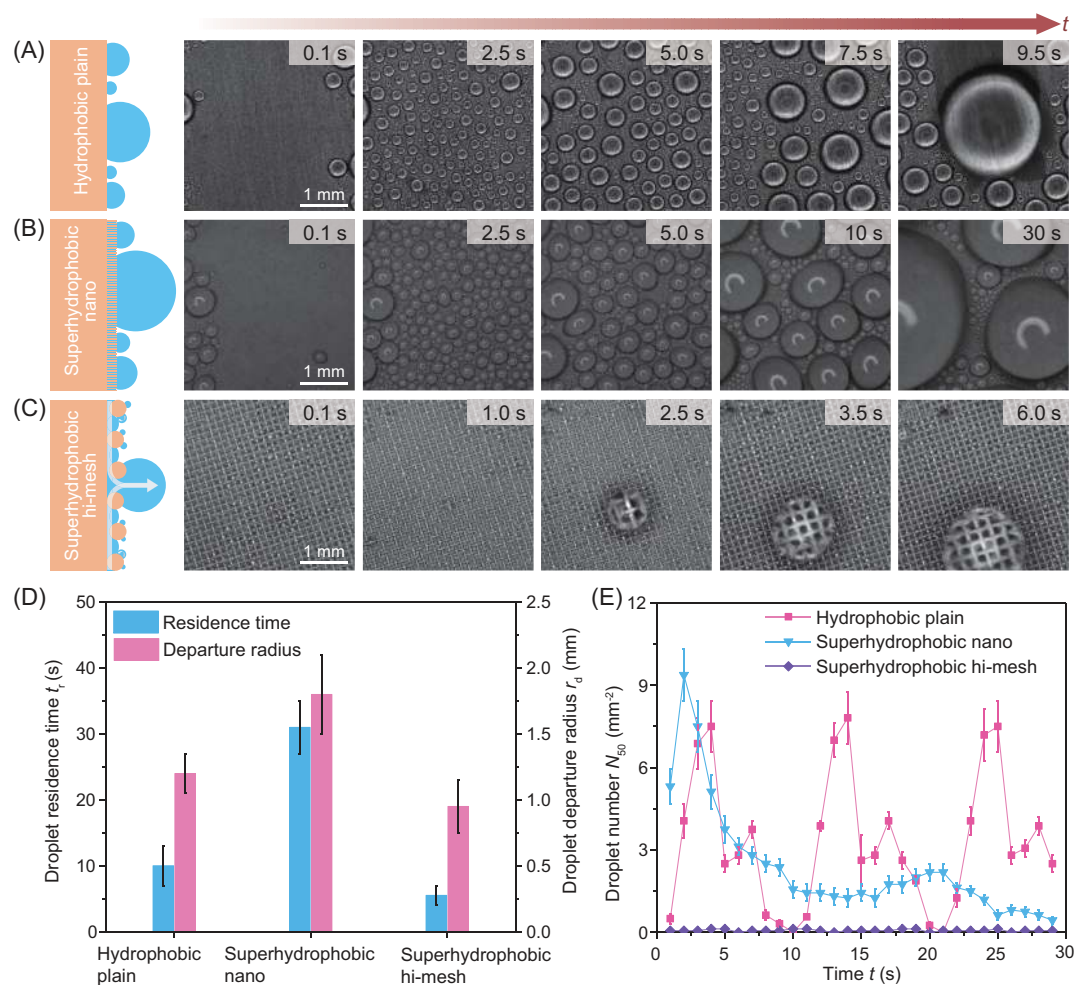


Figure 2. Condensation phenomenon under large surface subcooling ($\Delta T > 4.5$ K). (A) Time-lapse condensation figures on the hydrophobic plain surface: the surface is covered by growing droplets before they are removed by gravity. (B) Time-lapse condensation figures on the superhydrophobic nano surface: the pinned droplets on the nanostructures result in the flooding phenomenon (failure of superhydrophobicity). (C) Time-lapse condensation figures on the hi-mesh surface with $w/d = 2$: most of the surface area is covered by small droplets ($< 50 \mu\text{m}$) due to the rapid surface refreshing by sucking flow. (D) Histogram of droplet residence time t_r and departure radius r_d on the three test surfaces. Each datum is obtained by averaging the residence time and departure radius of 20 measured droplets on the test surface. (E) Time evolution of the number of large droplets N_{50} ($r > 50 \mu\text{m}$) on the three test surfaces.

number of small droplets on the superhydrophobic nano and hi-mesh surfaces (Fig. S5H) significantly reduces the thermal resistance of the liquid condensate. The increased surface refreshing and reduced thermal resistance for vapor condensation together can enhance condensation heat transfer under small surface subcooling. This droplet jumping condensation under small surface subcooling is indeed similar to earlier works on developing superhydrophobic nanostructured surfaces [25,26,30,39].

As the surface subcooling increases ($\Delta T > 4.5$ K), a significantly different condensation phenomenon is observed here for the first time on the superhydrophobic hi-mesh surfaces. Figure 2A–C shows the condensation phenomenon on the hydrophobic plain, superhydrophobic nano, and

superhydrophobic hi-mesh surfaces at a surface subcooling of 15 K, respectively. Compared to the dropwise condensation on the hydrophobic plain surface (Fig. 2A, also Movie S4) and flooding condensation on the superhydrophobic nano surface (Fig. 2B, also Movie S5), an unprecedented condensation mode of sucking flow is observed on the superhydrophobic hi-mesh surface (Fig. 2C, also Movie S6). At short times after droplet departure at 0.1 s, all three test surfaces are covered by lots of newly nucleated droplets. Such high-density small droplets can transfer heat more efficiently from the vapor to the surface [23,38]. However, the differences become apparent after 2.5 s: the droplets on the hydrophobic plain and superhydrophobic nano surfaces continuously grow and coalesce

with neighboring droplets to a bigger size to cover the surface, while most of the surface area on the superhydrophobic hi-mesh surface remains covered by the newly generated small droplets. Figure 2D quantitatively shows the residence time (from droplet formation to removal) and departure radius of droplets on the test surfaces. Compared to the droplets on the hydrophobic plain surface, the residence time of droplets on the superhydrophobic hi-mesh surfaces is reduced from 9.5 s to 6 s, which is only one-fifth of that on the superhydrophobic nano surface ($t_r = 30$ s). In addition, the droplet departure radius on the superhydrophobic hi-mesh surface (0.8–1.1 mm) is decreased to 80% of that on the hydrophobic plain surface (1.0–1.3 mm) and 53% of that on the superhydrophobic nano surface (1.5–2.1 mm). The significantly increased residence time and departure radius of droplets on the superhydrophobic nano surface are due to the strongly pinned droplet wetting state [26,40]. The reduced residence time of droplets on the hi-mesh surface is attributed to the rapid droplet growth through the sucking flow of liquid film in the interweaving channels, which greatly accelerates surface refreshing. Figure 2E shows the evolution of the density of large droplets with a radius of $> 50 \mu\text{m}$ on the three test surfaces. For dropwise condensation on the hydrophobic plain surface, the density of large droplets rapidly increases as new droplets nucleate and grow after the departure of old droplets (0–4 s). Due to the coalescence of large droplets, the density of large droplets reduces (4–5 s). As vapor further condenses on the exposed surface area caused by droplet coalescence, new droplets nucleate and grow, resulting in the density of large droplets increasing again (5–7 s). When the droplets grow large enough (1–1.2 mm) to be removed by gravity, the surface is refreshed and the density of large droplets greatly decreases (7–10 s). The repeated droplet cycle from nucleation to departure results in the periodic increase and decrease in the number of large droplets. Compared to the hydrophobic plain surface, the density of large droplets on the superhydrophobic nano surface increases similarly with the nucleation and growth of new droplets after the departure of old droplets (0–2 s). The further coalescence of droplets reduces the density of large droplets (2–30 s) until the droplets are removed by gravity.

Significantly different from the hydrophobic plain and superhydrophobic nano surfaces, the density of large droplets on the superhydrophobic hi-mesh surface remains very small over time (Fig. 2E). Such a small density of large droplets is attributed to both the droplet-to-film coalescence and film-to-liquid sucking flow on the superhydrophobic hi-mesh surfaces (Fig. 1C). The droplet-to-film

coalescence can rapidly remove the droplets on the mesh wires at a smaller size ($< 50 \mu\text{m}$) compared to the gravity-driven droplet removal size (1.0–1.3 mm) on the hydrophobic plain surface. The further film-to-droplet sucking flow between the substrate and woven mesh layer can effectively drain the liquid condensate accumulated in the interweaving channels in the form of falling droplets driven by gravity.

To further explore the effect of the hi-mesh structures on the condensation performance, Fig. 3 quantitatively shows the droplet behaviors on hydrophobic plain, superhydrophobic nano, and three superhydrophobic hi-mesh surfaces. Figure 3A shows the droplet size distribution on the five test surfaces at $\Delta T = 15$ K. The droplet counts were averaged over five images recorded during a droplet cycle. On the superhydrophobic hi-mesh surfaces, the number of small droplets ($< 50 \mu\text{m}$) has more than doubled while the number of large droplets ($> 50 \mu\text{m}$) is greatly decreased compared to that on the hydrophobic plain and superhydrophobic nano surfaces. The increased number of small droplets on the hi-mesh surfaces significantly reduces the thermal resistance of the condensate layer. Among the three superhydrophobic hi-mesh surfaces, the surface with $w/d = 3$ has the largest number of small droplets and the smallest number of large droplets, which renders the best condensation heat transfer characteristics. Figure 3B shows the surface coverage of the five test surfaces as a function of time after surface refreshing (droplet departure). Due to the droplet growth by coalescence with neighboring droplets, the surface coverage of the hydrophobic plain surface and superhydrophobic nano surfaces increases rapidly up to 60% and 80%, respectively, until being refreshed by the next droplet departure. However, the droplet coverage on the superhydrophobic hi-mesh surfaces is found to be kept at a small value (less than 40%) during the condensation process. Such a low surface coverage of the hi-mesh surfaces provides more fresh surface area for efficient vapor condensation. Figure 3C shows the droplet growth rate on the five test surfaces at a surface subcooling of 15 K. After droplet departure at 0 s, the average volume of new droplets on the fresh surface area is measured. At short times (< 1 s) after droplet departure, the small droplets grow by direct vapor condensation on the droplet surface. Once the droplets coalesce with adjacent droplets (> 1 s), droplet coalescence becomes the dominant mechanism for droplet growth, since the droplet growth contributed by direct vapor condensation decreases due to the increased thermal resistance between droplet surface and the substrate. The droplets on all three superhydrophobic hi-mesh surfaces have much larger

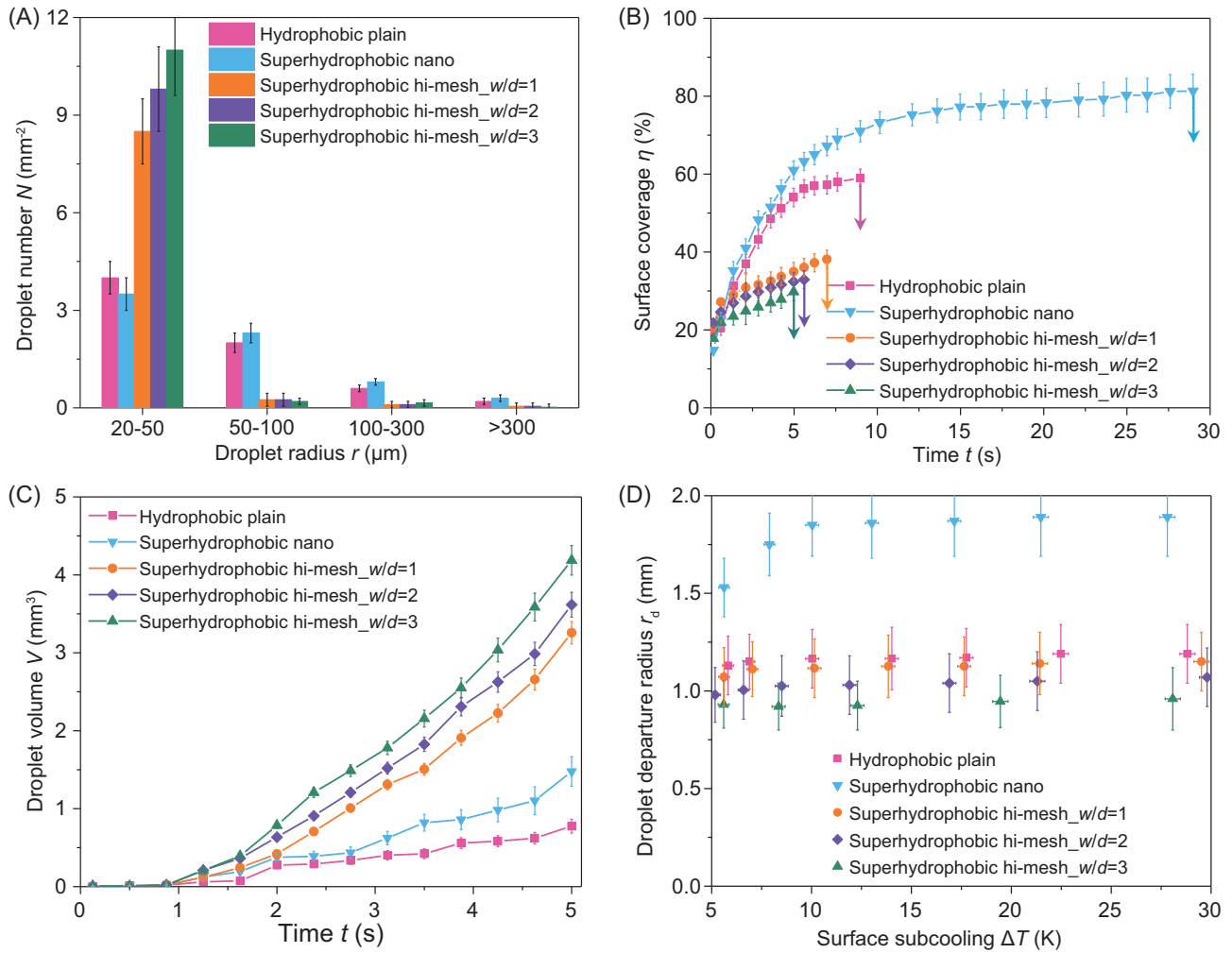


Figure 3. Droplet dynamic behaviors. (A) Histogram of droplet size distribution (averaged for a duration of 60 s of condensation) on the five test surfaces. A larger number of small droplets ($<50 \mu\text{m}$) on the hi-mesh surfaces reduces the thermal resistance of the liquid condensate layer. (B) Time evolution of surface coverage η from droplet formation to departure on the five test surfaces. The surface coverage is averaged for the measurements for three droplet cycles on the same surface. (C) Time evolution of the volume of growing droplets V showing the enhanced droplet growth on the hi-mesh surfaces. The droplet volume is the average for three measured droplets on the same surface. (D) Quantification of the departure radius of droplets r_d on the five test surfaces as a function of surface subcooling ΔT . The droplet departure radius is averaged for an interval of 60 s of condensation. The departure radius of droplets on the hi-mesh surfaces is decreased compared to that on the hydrophobic plain surface and superhydrophobic nano surface.

growth rates than those on the hydrophobic plain and superhydrophobic nano surfaces. More importantly, the superhydrophobic hi-mesh surfaces show an accelerated droplet growth rate (increased slope dV/dt with time t), which is significantly different from the reduced growth rate for growing droplets on other plain and structured surfaces [41–43]. Among the three hi-mesh surfaces, the hi-mesh surface with $w/d = 3$ has the largest droplet growth rate, which is five times that on the hydrophobic plain surface. Figure 3D shows the departure radius of droplets on the five test surfaces as a function of surface subcooling. As expected, the droplet departure radius on the vertical hydrophobic plain surface is maintained at 1.0–1.3 mm, which is comparable

to the capillary length of water [38]. Due to the increased surface adhesion caused by the pinned wetting state at large surface subcooling [26], the droplets on the superhydrophobic nano surface grow larger than 1.5 mm before being removed by gravity. For all the superhydrophobic hi-mesh surfaces, the droplet departure radius decreases to 0.8–1.1 mm and the smallest droplet departure radius is obtained on the hi-mesh surface with $w/d = 3$. The improved condensation characteristics under large surface subcooling, including faster droplet growth rate, smaller droplet departure radius, higher density of small droplets, and more frequent surface refreshing together provide great potential for sustained condensation heat transfer enhancement.

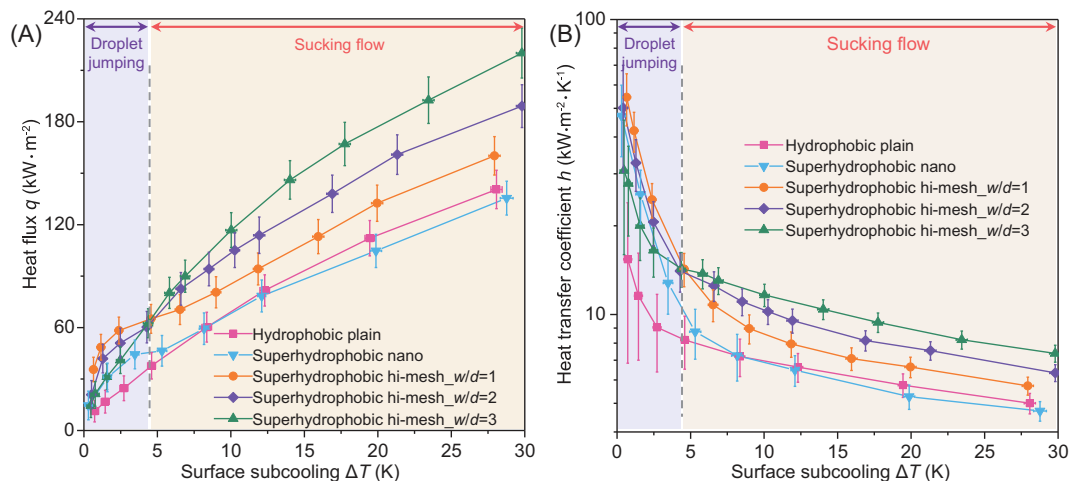


Figure 4. Condensation heat transfer performance. (A) Heat flux q and (B) heat transfer coefficient h on the five test surfaces as a function of surface subcooling ΔT , respectively. Based on the condensation characteristics, the heat transfer curves of superhydrophobic hi-mesh surfaces can be divided into two regimes: droplet jumping under small surface subcooling ($\Delta T < 4.5$ K) and sucking flow under large surface subcooling ($\Delta T > 4.5$ K). The change of condensation mode from droplet jumping to sucking flow is due to the droplet wetting transition from the suspended state to the immersed state. Enhanced condensation heat transfer in the droplet jumping regime is attributed to the increased surface refreshing. Heat transfer enhancement sustained under large surface subcooling is due to the sucking-flow-enhanced droplet growth and surface refreshing.

Figure 4A shows the condensation heat flux q as a function of surface subcooling ΔT on the five test surfaces. Dropwise condensation heat transfer on the hydrophobic plain surface and superhydrophobic nano surface are also shown here for comparison. At each surface subcooling, the heat flux on the three hi-mesh surfaces is significantly enhanced in comparison with the hydrophobic plain copper surface. More interestingly, the unprecedented sustained heat transfer enhancement is achieved over a wide range of surface subcooling, up to 30 K, compared to that on the superhydrophobic nano surface. Obviously, there exists a transition point at a surface subcooling of 4.5 K, where the heat flux curves of the superhydrophobic hi-mesh surfaces can be divided into two regimes based on different condensation phenomena: droplet jumping ($\Delta T < 4.5$ K) and sucking flow ($\Delta T > 4.5$ K). The transition of condensation mode from jumping droplet condensation to sucking flow condensation is attributed to the wetting transition of condensed droplets from the suspended Cassie state to the immersed Wenzel state caused by droplet nucleation within the nanostructures under large surface subcooling [26]. On the superhydrophobic nano surface, when the surface subcooling increases, the nucleation size of droplets significantly decreases while the nucleation site density greatly increases, which results in a change of droplet removal from the self-propelled jumping mode to the gravity-driven sliding mode. It is worth noting that the wetting transition on the hi-mesh

surfaces does not lead to the flooding phenomena that have often been observed to occur on other micro/nanostructured superhydrophobic surfaces developed for condensation enhancement [25,26,44].

By further comparing the heat flux curves of the three superhydrophobic hi-mesh surfaces, the largest heat transfer enhancement in the two regimes appears on different surfaces: the largest heat transfer enhancement in the droplet jumping regime is obtained on the superhydrophobic hi-mesh surface with $w/d = 1$ while the highest heat flux in the sucking flow condensation regime is achieved on the hi-mesh surface with $w/d = 3$. This is because the superhydrophobic hi-mesh surface with $w/d = 1$ provides smaller and denser micropores for rapid droplet jumping under small surface subcooling (< 4.5 K) while the hi-mesh surface with $w/d = 3$ has the lower flow resistance of film-to-droplet sucking under large surface subcooling (> 4.5 K). Compared to that on the hydrophobic plain surface, Fig. 4B shows that 254% and 74% higher heat transfer coefficients are achieved on the hi-mesh surface with $w/d = 1$ in the droplet jumping regime at surface subcooling of 0.7 K and 4.5 K, respectively. Such a significant enhancement can be understood from the enhanced surface refreshing by the reduced droplet departure size: the jumping droplets on the hi-mesh surfaces can rapidly leave the surface with a smaller size ($r < 300 \mu\text{m}$) while the droplets on the hydrophobic plain surface keep growing to a larger size ($r > 1 \text{ mm}$) until being able to be removed



Figure 5. Far-reaching technological applications. Superhydrophobic hi-mesh surfaces as demonstrated in this work to sustain unprecedented condensation heat transfer enhancement over a wide range of surface subcooling can greatly push the frontier of bio-inspired water-repellent surfaces into practical phase-change applications related to energy and water systems.

by gravity. More importantly, compared to that on the hydrophobic plain surface, 70% and 53% higher heat transfer coefficients are obtained on the hi-mesh surface with $w/d = 3$ at surface subcooling of 8.3 K and 28.1 K, respectively. Such a significant and sustained condensation heat transfer enhancement is attributed to a new condensation mode: sucking flow condensation on the superhydrophobic hi-mesh surfaces (more condensation heat transfer results on various structured surfaces are given for comparison in Supplementary Note S6, available at NSR online).

CONCLUSION

Sustained enhanced condensation on superhydrophobic hi-mesh surfaces as demonstrated above is not only of fundamental scientific interest, revealing the novel sucking-flow-enhanced liquid removal and surface refreshing; it also tackles the long-standing challenge in pushing the frontier of superhydrophobic surfaces into practical energy and water applications. Inspiration from non-wetting structures in nature, such as lotus leaves, water striders, and butterfly wings, has led to exciting improvements in water-repellent surfaces for environmental and biological applications (Fig. 5), such as self-cleaning, anti-corrosion, anti-bacterial, oil-liquid separation, and drag reduction. Most of these surfaces are, however, still plagued with problems that restrict their practical applications in phase-change enhancement: limited surface refreshing due to nucleation-induced flooding

phenomenon, intrinsic trade-offs of droplet growth and removal, and expensive manufacturing processes. In addition, hydrophobic coating plays a key role in increasing surface repellency during condensation. To reduce the additional thermal resistance of hydrophobic coatings, a self-assembled coating that has been demonstrated to maintain good condensation performance after 500 h of operation [45] is used in this study to promote dropwise condensation. Bridging the gap between the water-repellent surfaces and high-performance phase-change processes, such low-cost superhydrophobic hi-mesh surfaces developed in this work are readily available to be deployed at scale for a wide range of energy and water applications (Fig. 5). For example, high-efficiency phase-change heat transfer is the key to high-performance heat exchangers, which are critical to power generation, water desalination and harvesting, air-conditioning, and thermal management of electronics. For the thermally driven water desalination systems that account for over 40% of the world's desalination capacity, the overall efficiency of heat exchangers can be improved 1.6 times and the product water cost could be reduced by as much as 35% when the dominant filmwise condensation is replaced by the more efficient dropwise condensation heat transfer. Efficient condensation in passive cooling devices such as heat pipes and vapor chambers can reduce the thermal resistance for heat dissipation and improve the lifetime and reliability of electronics.

METHODS

Fabrication of superhydrophobic hi-mesh surfaces

Due to the broad applications of copper in thermal and energy systems, high-purity copper (99.9% purity) is used to fabricate the test samples in this work. Commercially available woven copper meshes (from TWP Inc) with a wire diameter of 65 μm and the spacing widths of 65, 130, and 195 μm are used as the starting materials. Superhydrophobic hi-mesh surfaces are fabricated by bonding woven copper mesh onto the plain copper substrate through the diffusion bonding method in a vacuum oven at 250°C for 4 h. Copper oxide nanostructures are then synthesized on the exposed surface of the substrate and mesh wires by the self-limiting chemical oxidation method, where the sample is dipped into an alkaline solution composed of NaClO_2 , NaOH , $\text{Na}_3\text{PO}_4 \cdot 12\text{H}_2\text{O}$ and DI water (3.75: 5: 10: 100 wt. %) at a temperature of 80°C for 20 min. Hydrophobic functionalization of the test surfaces is obtained by dipping the sample into an ethanol solution of

2.5 mM *n*-octadecanethiol (96% *n*-octadecyl mercaptan, Sigma-Aldrich) at a temperature of 70°C for 1 h. Further details on the surface fabrication are given in Supplementary Note S1, available at *NSR* online.

Experimental system for condensation heat transfer

We have built a custom-made experimental set-up with *in situ* visualization capability for measuring condensation heat transfer performance. The set-up consists of a condensation chamber, a steam generator, a chilled water bath, a vacuum pump, and a data acquisition subsystem. The DI water in the steam generator is heated by an electric heater to supply water vapor into the condensation chamber, which can be adjusted by a direct-current regulator (Agilent, N5771A). The water vapor generated in the steam generator flows into the condensation chamber through a connecting pipe. To prevent vapor condensation on the inner wall of the pipe, the pipe is covered with adjustable heating tape (Omega, HTWC 101-004). A pressure transducer (Omega, PX409-050AI) and temperature transducers (T-type thermocouples) are instrumented in the condensation chamber. Test surfaces are mounted vertically in the condensation chamber. To obtain the surface temperature, three thermocouples are installed in parallel in the condensing block to measure the temperature distribution. To dissipate the latent heat from vapor condensation, a chilled water bath (Thermo Electron Corporation, HAAKE Phoenix II) is used to pump the cooling water to flow through the condensing block. A flow meter (Proteus Industries, 08004SN1) is used to monitor the cooling water to determine the heat flux using a data acquisition system (Agilent, 34970A). To remove the non-condensable gases in the condensation chamber, a vacuum pump (Edwards, RV8) is integrated into the vacuum line to pump down the experimental system before the DI water is poured into the steam generator. During condensation heat transfer measurements, the concentration of non-condensable gas in the condensation chamber is ~2.5%. The condensation characteristics of various test samples are visualized using a high-speed camera (Photron FASTCAM SA4) through a transparent window. A more detailed description of the experimental system is given in Supplementary Note S3, available at *NSR* online.

SUPPLEMENTARY DATA

Supplementary data are available at [NSR](#) online.

FUNDING

This work was supported by the financial support from the USDA National Institute of Food and Agriculture (USDA/NIFA 2018-67003-27407).

Conflict of interest statement. None declared.

REFERENCES

- Parker AR and Lawrence CR. Water capture by a desert beetle. *Nature* 2001; **414**: 33–4.
- Prakash M, Quere D and Bush JWM. Surface tension transport of prey by feeding shorebirds: the capillary ratchet. *Science* 2008; **320**: 931–4.
- Zheng YM, Bai H and Huang ZB *et al.* Directional water collection on wetted spider silk. *Nature* 2010; **463**: 640–3.
- Song M, Ju J and Luo S *et al.* Controlling liquid splash on superhydrophobic surfaces by a vesicle surfactant. *Sci Adv* 2017; **3**: e1602188.
- Chaudhury MK and Whitesides GM. How to make water run uphill. *Science* 1992; **256**: 1539–41.
- Wang JZ, Zheng ZH and Li HW *et al.* Dewetting of conducting polymer inkjet droplets on patterned surfaces. *Nat Mater* 2004; **3**: 171–6.
- Huang JH, Juszkiewicz M and Jeu WH *et al.* Capillary wrinkling of floating thin polymer films. *Science* 2007; **317**: 650–3.
- Wong TS, Kang SH and Tang SK *et al.* Bioinspired self-repairing slippery surfaces with pressure-stable omniphobicity. *Nature* 2011; **477**: 443–7.
- Vakarelski IU, Patankar NA and Marston JO *et al.* Stabilization of Leidenfrost vapour layer by textured superhydrophobic surfaces. *Nature* 2012; **489**: 274–7.
- Gao X and Jiang L. Water-repellent legs of water striders. *Nature* 2004; **432**: 36.
- Wisdom KM, Watson JA and Qu XP *et al.* Self-cleaning of superhydrophobic surfaces by self-propelled jumping condensate. *Proc Natl Acad Sci USA* 2013; **110**: 7992–7.
- Schutzius TM, Jung S and Maitra T *et al.* Spontaneous droplet trampolining on rigid superhydrophobic surfaces. *Nature* 2015; **527**: 82–5.
- Wang Q, Yao X and Liu H *et al.* Self-removal of condensed water on the legs of water striders. *Proc Natl Acad Sci USA* 2015; **112**: 9247–52.
- Tuteja A, Choi W and Ma ML *et al.* Designing superoleophobic surfaces. *Science* 2007; **318**: 1618–22.
- Lu Y, Sathasivam S and Song J *et al.* Robust self-cleaning surfaces that function when exposed to either air or oil. *Science* 2015; **347**: 1132–5.
- Bird JC, Dhiman R and Kwon HM *et al.* Reducing the contact time of a bouncing drop. *Nature* 2013; **503**: 385–8.
- Liu J, Guo H and Zhang B *et al.* Guided self-propelled leaping of droplets on a micro-anisotropic superhydrophobic surface. *Angew Chem Int Ed* 2016; **55**: 4265–9.
- Cheng Y-T and Rodak DE. Is the lotus leaf superhydrophobic? *Appl Phys Lett* 2005; **86**: 144101.

19. Mouterde T, Lehoucq G and Xavier S *et al.* Antifogging abilities of model nanotextures. *Nat Mater* 2017; **16**: 658–63.
20. He M, Li H and Wang J *et al.* Superhydrophobic surface at low surface temperature. *Appl Phys Lett* 2011; **98**: 093118.
21. Kreder MJ, Alvarenga J and Kim P *et al.* Design of anti-icing surfaces: smooth, textured or slippery? *Nat Rev Mater* 2016; **1**: 15003.
22. Kim H, Yang S and Rao SR *et al.* Water harvesting from air with metal-organic frameworks powered by natural sunlight. *Science* 2017; **356**: 430–4.
23. Cho HJ, Preston DJ and Zhu Y *et al.* Nanoengineered materials for liquid–vapour phase-change heat transfer. *Nat Rev Mater* 2016; **2**: 16092.
24. Daniel S, Chaudhury MK and Chen JC. Past drop movements resulting from the phase change on a gradient surface. *Science* 2001; **291**: 633–6.
25. Miljkovic N, Enright R and Nam Y *et al.* Jumping-droplet-enhanced condensation on scalable superhydrophobic nanostructured surfaces. *Nano Lett* 2013; **13**: 179–87.
26. Wen RF, Li Q and Wu JF *et al.* Hydrophobic copper nanowires for enhancing condensation heat transfer. *Nano Energy* 2017; **33**: 177–83.
27. Boreyko JB and Chen CH. Self-propelled dropwise condensate on superhydrophobic surfaces. *Phys Rev Lett* 2009; **103**: 184501.
28. Park KC, Kim P and Grinthal A *et al.* Condensation on slippery asymmetric bumps. *Nature* 2016; **531**: 78–82.
29. Dai X, Sun N and Nielsen SO *et al.* Hydrophilic directional slippery rough surfaces for water harvesting. *Sci Adv* 2018; **4**: eaaq0919.
30. Wen RF, Xu SS and Ma XH *et al.* Three-dimensional superhydrophobic nanowire networks for enhancing condensation heat transfer. *Joule* 2018; **2**: 269–79.
31. He M, Zhou X and Zeng XP *et al.* Hierarchically structured porous aluminum surfaces for high-efficient removal of condensed water. *Soft Matter* 2012; **8**: 6680–3.
32. Lv J, Song Y and Jiang L *et al.* Bio-inspired strategies for anti-icing. *ACS Nano* 2014; **8**: 3152–69.
33. Zhang S, Huang J and Cheng Y *et al.* Bioinspired surfaces with superwettability for anti-icing and ice-phobic application: concept, mechanism, and design. *Small* 2017; **13**: 1701867.
34. Gao X, Zhou J and Du R *et al.* Robust superhydrophobic foam: a graphdiyne-based hierarchical architecture for oil/water separation. *Adv Mater* 2016; **28**: 168–73.
35. Ryu S, Sen P and Nam Y *et al.* Water penetration through a superhydrophobic mesh during a drop impact. *Phys Rev Lett* 2017; **118**: 014501.
36. Wen R, Xu S and Lee Y-C *et al.* Capillary-driven liquid film boiling heat transfer on hybrid mesh wicking structures. *Nano Energy* 2018; **51**: 373–82.
37. Wen RF, Xu SS and Yang RG. Micromesh-covered superhydrophobic surfaces for efficient condensation heat transfer. *Thermal and Thermomechanical Phenomena in Electronic Systems (ITherm), 2017: 16th IEEE Intersociety Conference*. IEEE, Orlando, FL, USA: Curran Associates, Inc. 2017, 220–6.
38. Rose JW. Dropwise condensation theory and experiment: A review. *Proc Inst Mech Eng A* 2002; **216**: 115–28.
39. Hou YM, Yu M and Chen XM *et al.* Recurrent filmwise and dropwise condensation on a beetle mimetic surface. *ACS Nano* 2015; **9**: 71–81.
40. Wen RF, Lan Z and Peng BL *et al.* Wetting transition of condensed droplets on nanostructured superhydrophobic surfaces: coordination of surface properties and condensing conditions. *ACS Appl Mater Interfaces* 2017; **9**: 13770–7.
41. Sharma CS, Combe J and Giger M *et al.* Growth rates and spontaneous navigation of condensate droplets through randomly structured textures. *ACS Nano* 2017; **11**: 1673–82.
42. Li GQ, Alhosani MH and Yuan SJ *et al.* Microscopic droplet formation and energy transport analysis of condensation on scalable superhydrophobic nanostructured copper oxide surfaces. *Langmuir* 2014; **30**: 14498–511.
43. Beysens D. Dew nucleation and growth. *Compt Rendus Phys* 2006; **7**: 1082–100.
44. Narhe RD and Beysens DA. Nucleation and growth on a superhydrophobic grooved surface. *Phys Rev Lett* 2004; **93**: 076103.
45. Vemuri S and Kim KJ. An experimental and theoretical study on the concept of dropwise condensation. *Int J Heat Mass Transfer* 2006; **49**: 649–57.